REPORT DOCUMENTATION PAGE	Form Approved OMB No. 0704-0188

1. REPORT DATE (DD-MM-YYYY)	2. REPORT TYPE	3. DATES COVERED (From - To)
09-02-2012	Journal Article	

4. TITLE AND SUBTITLE
Can Dynamic Bubble Templating Play a Role in Corrosion Product Morphology

5a. CONTRACT NUMBER

5b. GRANT NUMBER

5c. PROGRAM ELEMENT NUMBER
0601153N

6. AUTHOR(S)
T.L Gerke, Kirk Scheckel, Richard I. Ray, Brenda J. Little

5d. PROJECT NUMBER

5e. TASK NUMBER

5f. WORK UNIT NUMBER
73-9576-01-5

7. PERFORMING ORGANIZATION NAME(S) AND ADDRESS(ES)
Naval Research Laboratory
Oceanography Division
Stennis Space Center, MS 39529-5004

8. PERFORMING ORGANIZATION REPORT NUMBER
NRL/JA/7330-11-0717

9. SPONSORING/MONITORING AGENCY NAME(S) AND ADDRESS(ES)
Office of Naval Research
One Liberty Center
875 North Randolph Street, Suite 1425
Arlington, VA 22203-1995

10. SPONSOR/MONITOR'S ACRONYM(S)
ONR

11. SPONSOR/MONITOR'S REPORT NUMBER(S)

12. DISTRIBUTION/AVAILABILITY STATEMENT
Approved for public release, distribution is unlimited.

20120213028

13. SUPPLEMENTARY NOTES

14. ABSTRACT
Dynamic templating as a result of cathodic hydrogen gas production is suggested as a possible mechanism for the formation of tube-like corrosion products on an unlined cast iron pipe in a drinking water distribution system. Mounds of corrosion product, with protruding tubes and freestanding tubes, were observed within a single 30 cm section of piping. Internal morphologies for all shapes were texturally complex although mineralogically simple, composed of two iron oxide/oxyhydroxides minerals: α-FeOOH (goethite) and Fe_3O_4 (magnetite). Static templating by either microorganisms or minerals was rejected as a possible mechanism for tube formation in this study.

15. SUBJECT TERMS
iron, morphologies, tube-shaped corrosion

16. SECURITY CLASSIFICATION OF:			17. LIMITATION OF ABSTRACT	18. NUMBER OF PAGES	19a. NAME OF RESPONSIBLE PERSON
a. REPORT	b. ABSTRACT	c. THIS PAGE			Richard I. Ray
Unclassified	Unclassified	Unclassified	UU	7	19b. TELEPHONE NUMBER (Include area code) 228-688-4690

Can Dynamic Bubble Templating Play a Role in Corrosion Product Morphology?

T.L. Gerke,‡,* K.G. Scheckel,** R.I. Ray,*** and B.J. Little***

ABSTRACT

Dynamic templating as a result of cathodic hydrogen gas production is suggested as a possible mechanism for the formation of tube-like corrosion products on an unlined cast iron pipe in a drinking water distribution system. Mounds of corrosion product, with protruding tubes and freestanding tubes, were observed within a single 30 cm section of piping. Internal morphologies for all shapes were texturally complex although mineralogically simple, composed of two iron oxide/oxyhydroxides minerals: α-FeOOH (goethite) and Fe_3O_4 (magnetite). Static templating by either microorganisms or minerals was rejected as a possible mechanism for tube formation in this study.

KEY WORDS: iron, μ-x-ray diffraction, μ-x-ray fluorescence mapping, morphologies, tube-shaped corrosion

INTRODUCTION

Unlined cast iron pipes (major alloyants carbon and silicon), common in drinking water distribution systems (DWDS) worldwide, are highly susceptible to general (interchangeable anodes and cathodes) and localized corrosion (fixed anodes) with accumulations of iron corrosion products.[1-3] The predominant corrosion product morphology is mound-shaped (often called a tubercle); however, other morphologies including flutes or cones, mounds with protruding tubes, and free-standing tubes have been observed.[4]

Research on the characteristics and mechanism(s) of corrosion product formation and growth has focused on mounds because of their prevalence. Working with iron corrosion products in cooling water systems, Herro[5] defined the accumulations as structurally complex with distinct regions, i.e., a core (C), a hard shell layer (HSL), and a surface layer (SL). The stratification and mineralogy of these distinct regions are remarkably consistent in different water chemistries.[5-7] Mechanisms of formation and growth are reasoned to be a result of iron release at the anode, followed by precipitation in close proximity to the anode.[3] Some mechanisms for mound formation indicate a spatial relationship between anodic sites and mound formation, and a connection between the height of the mound and the depth of the resulting pit.[8-9] That relationship is not always obvious in DWDS where mounds can accumulate at locations with little evidence of pit formation.[7] Smith and McEnaney[10] indicated corrosion product buildup as a result of both pitting and general corrosion. Investigators have demonstrated bacteria and bacterial stalks within core regions.[7] However, they[7] concluded that bacteria are not the only cause of corrosion product accumulation and that the presence of mounds/tubercles cannot be used to conclude the involvement of bacteria or microbiologically influenced corrosion (MIC).

It has been proposed by Baylis[11] that flutes or cones formed in a manner similar to mounds, but as the iron precipitated, the corrosion product was elon-

Submitted for publication September 2, 2011; in revised form, September 12, 2011.
‡ Corresponding author. E-mail: Tammie.Gerke@uc.edu.
* Department of Geology, University of Cincinnati, Cincinnati, OH 45221.
** U.S. Environmental Protection Agency, ORD, NRMRL, LRPCD 26 W. Martin Luther King Drive, Cincinnati, OH 45268.
*** Naval Research Laboratory, Stennis Space Center, MS 39529.

ISSN 0012-9312 (print), 1938-159X (online)
12/000027/$5.00+$0.50/0

gated in the direction of water flow. However, no physicochemical characterization of the flutes/cones or tubes was presented. He proposed though that tube-shaped corrosion product formation was linked to the water calcium saturation index but provided no explanation regarding this relationship.[11]

Tube-shaped features are common in natural, quiescent environments, ranging in size from a few millimeters (soda straws in caves) to meters (chimneys at hydrothermal vents)[12] and form as a result of static and dynamic templating. Static templating is a common process where precipitating minerals accumulate on artificial or natural substrata whose shape controls the morphology of the precipitate. Static templating requires flowing waters. Dynamic templating is less common because tube growth requires a constant and fairy uniform feature for precipitating material. Main portions of a DWDS piping have steady flow, but residential portions experience daily stagnation.

In the following study, physicochemical data were examined to evaluate the possibility of static and dynamic templating processes for creating tube-shaped iron corrosion products in DWDS. Samples were examined using powder x-ray diffraction (XRD) and x-ray fluorescence (XRF) in addition to synchrotron-based μ-XRD and μ-XRF mapping.

EXPERIMENTAL PROCEDURES

Sample Selection and Preparation

An unlined cast iron DWDS pipe section (approximately 30 cm long by 15 cm inner diameter) was obtained from a drinking water utility in the northeastern United States. The pipe was cut in half using a band saw. Iron corrosion products were harvested from one half of the pipe for powder XRD and XRF analyses. Digital images of tubes were obtained from one half of the pipe and the elemental composition of the unlined iron pipe was determined using electron scanning electron microscopey (ESEM) previously described by Ray and Little.[13]

Bulk Powder X-Ray Diffraction and X-Ray Fluorescence

Approximately 0.2 g to 3.0 g of solids from areas of interest were extracted with metal spatulas from C, HSL, and SL of representative iron corrosion products. The solids were ground by hand, with an agate mortar and pestle, until they passed through a stainless steel 200 (75 μm) mesh sieve. Samples were processed for bulk powder XRD and XRF following the protocol of Gerke, et al.[14]

All samples were analyzed using a Siemens D-500† automated diffractometer system using a Cu Ka radiation at 30 mA and 40 kV. The 2Θ ranged from 5° to 70°, with a 0.02° step, and a 2 s count time at each step. Crystalline phase identifications were made on the basis of peak position and peak intensities using the American Mineralogist Crystal Structure Database[15] and the Mineral Database[16] (http://rruff.geo.arizona.edu/AMS/amcsd.php, http://webmineral.com/).

Scanning Electron Microscopy Analysis

Iron corrosion products of sample T4 were examined using ESEM coupled with energy-dispersive spectroscopy (EDS) as previously described by Ray, et al.[7]

Synchrotron-Based μ-XRD and μ-XRF Mapping

One half of the pipe was embedded in Buehler Epo Thin† low-viscosity epoxy. Mounds with protruding tubes and tubes were cut out of the epoxy. These were mounted on quartz slides, cut, polished to an average thickness of 35 μm and digitally imaged. A mound and tube from the same sample were used for synchrotron-based μ-XRD and μ-XRF mapping techniques. Colors of the iron phases were determined visually according to Cornell and Schwartmann.[17] X-ray μ-beam studies (fluorescence and diffraction spectroscopy) were performed at XOR/PNC 20 BM-B of the Advanced Photon Source, Argonne National Laboratory (Argonne, IL) under standard operating conditions (7 GeV operation and ring current of 101 mA in top-up mode). Digital images of the representative mound and tube were used to determine the locations for μ-XRF elemental maps and corresponding μ-XRD analyses. μ-XRF maps were recorded for Ca, Cr, Cu, Fe, Mn, Ni, and Zn. Relative elemental concentrations are shown using a color scale in which dark blue represents low concentrations and red represents comparatively higher concentrations. A MAR 165† CCD (μ-XRD) studies and points of interest were chosen based on location within the iron corrosion product and color. The CCD detector was positioned at approximately 200 mm from the sample and two-dimensional μ-XRD patterns were collected for 300 s at 15 kV with a wavelength of 0.8265 Å. Two-dimensional diffractograms (2D Debye Scherrer rings) were converted to one-dimensional 2Θ scans using the Fit2D† software.[18]

RESULTS

Description of Pipe and Corrosion Products

Corrosion products in the form of mounds, mounds with protruding tubes, and free-standing tubes were observed around the circumference of the pipe (Figure 1). The structure of tubes, their relationship to mounds, and the variability of that relationship is demonstrated in Figure 2. A free-standing tube (cut parallel to long axis) was composed of vertically stacked, alternating layers of C and HSL (Figure 2[a]). A tube protruding from a mound (cut parallel

† Trade name.

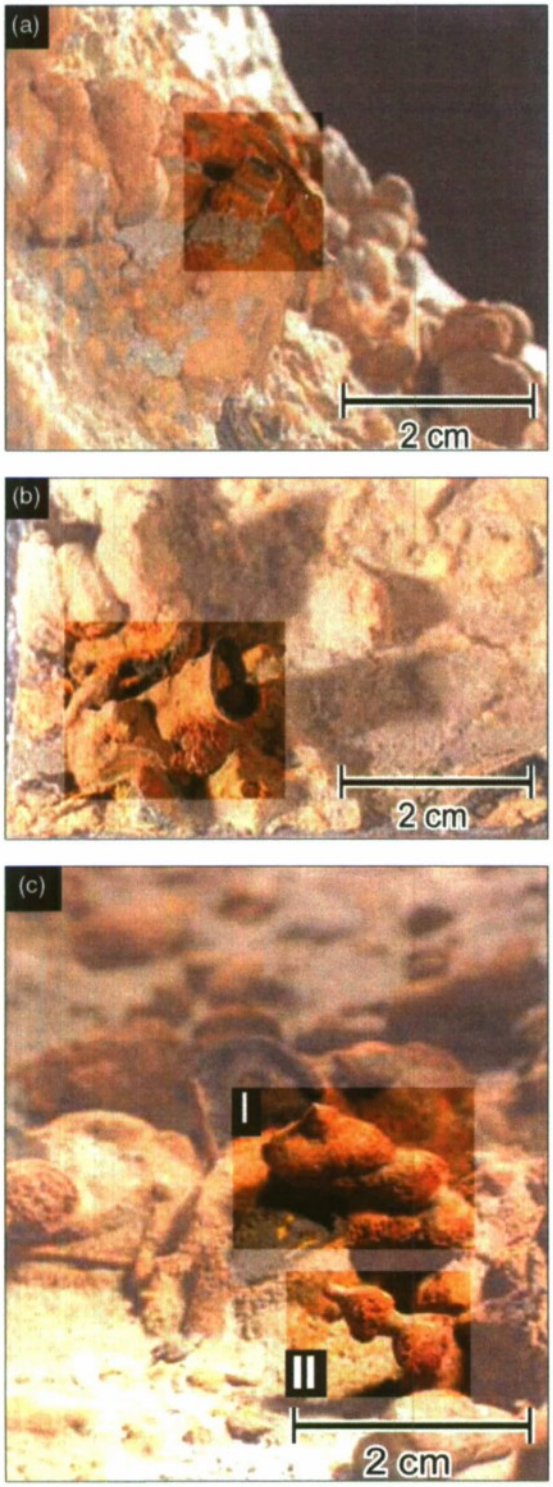

FIGURE 1. *Digital images of corrosion products. Tubes are highlighted.*

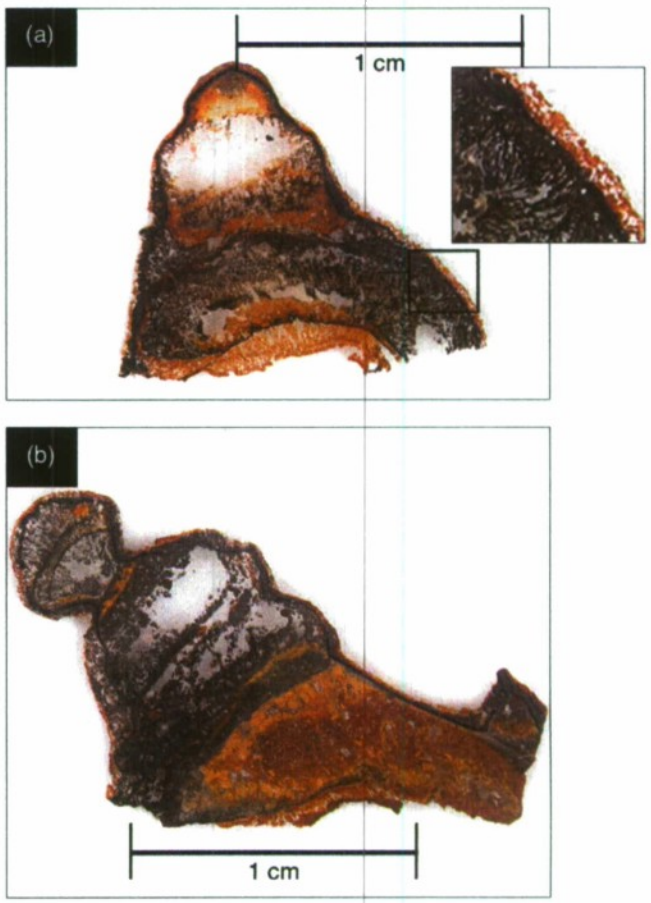

FIGURE 2. *Cross sections of corrosion products mounted on quartz slides and polished to an average thickness of 35 μm: (a) free-standing tube cut parallel to the long axis and (b) mound with tube cut parallel to the long axis of the tube. Enlargement showing details of HSL and SL uniformly encasing corrosion products.*

to its long axis) constricted (tapered) and then broadened before closing completely (Figure 2[b]). In all cases a thick black HSL covered by a red SL encased the tubes and mounds (enlargement in Figure 2[b]). A cm-sized feature was composed of two tubes and two mounds that had grown together (Figure 3). A large black tube, dominating the upper portion of the image was growing from the filamentous-textured, yellowish red-brown material mound. The smaller micro-sized mound and tube, indicated in boxes, were examined in detail (Figures 4 and 5).

Characteristics of a Mound

The internal structure of a 5 cm mound consisted of C dominated by yellowish-red brown material, primarily α-FeOOH (goethite) with moderate amounts of metallic luster Fe_3O_4 (magnetite), and trace amounts of $CaCO_3$ (calcite). In addition, the core was marbled with black non-metallic luster Fe_3O_4, minor amounts of α-FeOOH, and trace amounts of $CaCO_3$. The uppermost portion of C consisted of a thick layer of black non-metallic luster Fe_3O_4, covered by a discontinuous hard shell layer of black Fe_3O_4 with a metallic luster and moderate amounts of $CaCO_3$ and trace amounts of α-FeOOH. A discontinuous yellowish red SL consisted of moderate amounts of γ-FeOOH (lepidocrocite), Fe_3O_4, $CaCO_3$, and trace amounts of α-FeOOH, SiO_2 (quartz) and S. Iron concentrations were highest

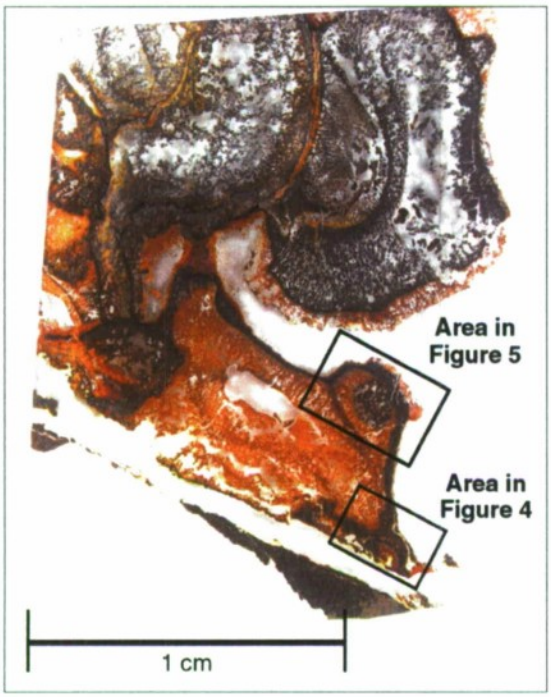

FIGURE 3. *Large black tube originating from red mound. Small mound and small tube (indicated in boxes) and examined in detail in Figures 4 and 5, respectively.*

and Mn and Ca were lowest in the core and associated veinlets. The HSL had the highest Ca concentrations, and the SL has the highest Pb, Mn, and Zn but the lowest Cu concentrations. Ni and Cr concentrations were below detection for all regions.

The internal structure of a 0.25 cm mound was similar. C1 (Figure 4, points 2 and 3) was composed of reddish brown α-FeOOH. The HSL of black metallic and non-metallic luster material was composed of Fe_3O_4 with moderate amounts of α-FeOOH at point 4. Covering the HSL was a thin surface layer of filamentous-textured, reddish brown material. The fine scale distributions of Ca, Cr, Cu, Fe, Mn, Ni, and Zn indicated that the concentrations of Cr, Cu, and Zn were very low (data not presented) for all regions of the corrosion product. The lower (C1) and upper (C2) core regions of the mound were composed primarily of Fe and trace amounts of Ni. The lower-most shell (HSL1) contained the highest concentration of Fe and moderate amounts of Ni. The outer shell (HSL2) had the same elemental distribution as HSL1. SL material was composed predominantly of Ca with lesser amounts of Fe and Ni.

Characteristics of Tubes

The micro-sized tube, oriented with its long axis perpendicular to the image, had an internal morphology C1 of filamentous-textured black material with a non-metallic luster, encircled by filamentous-textured reddish to yellowish brown material (C2) (Figure 5). C1 of the tube was composed primarily of Fe_3O_4 with minor to trace amounts of α-FeOOH (Figure 5, points 3 through 5) and C2 of α-FeOOH with minor to trace amounts of Fe_3O_4 (Figure 5, points 2 and 6). All parts of this corrosion product were enclosed by a thin layer of metallic luster black Fe_3O_4 with minor to trace amounts of α-FeOOH (points 1 and 7, Figure 5, HSL). This is all overlain by a filamentous-textured reddish brown SL with some locations having black material with a non-metallic luster located at the outer edges. The in situ synchrotron μ-XRF mapping of C1 showed that it was composed of Fe, Ni, and minor amounts of Mn (Figure 5). C2 and HSL were also composed of Fe and lesser amounts of Ni and Mn. The SL was composed primarily of Ca with some Ni and Mn.

DISCUSSION

A relationship between the calcite saturation index of water and the formation of tube-shaped corrosion products was proposed by Baylis.[11] In that work, calcite was the main accessory phase associated with cm-sized mounds, and a discrete layer of calcium was associated with the smaller 0.25 cm-sized mound and 0.50 cm-sized tube-shaped corrosion products, indicating that the corrosion products formed in water near or exceeding the calcite saturation index. In the present study, there was no relationship between corrosion products and calcium.

In DWDS, the most likely static templates are minerals and microorganisms. Typical mineral phases associated with iron corrosion products include α- or γ-FeOOH and Fe_3O_4 and accessory phases such as $FeCO_3$ (siderite) and $CaCO_3$.[4-5,11,19-23] In addition, as metal ions from the pipe wall are released into the drinking water, they may form atypical, elongate mineral phases. Based on the pipe wall composition and the chemical analyses of the tube-shaped corrosion products, no unique mineral phases were identified in this study. The general size of a single iron oxide/oxyhydroxide or calcite crystal in corrosion products is microns, and none have an elongate cylindrical morphology required for templating surfaces producing cm-sized features.

Microorganisms, present in all DWDS,[24] can have rod-shaped morphologies or could produce filaments, sheaths, or stalks, which could produce static templates for tube-shaped features. For example, *Leptothrix ochracea* produces hollow sheaths (microtubes) that range in length from 10 μm to 200 μm and have an outer diameter of 1.4 μm.[25] ESEM analysis of corrosion products in this study, though, did not detect microorganisms or microbial features that could serve as templates. More importantly, static templating from the presence of microorganisms produces structures that are orders of magnitude smaller than any of the tubes observed in the unlined cast iron pipe.

One potential mechanism for tube formation is precipitation of anodically produced iron particulate

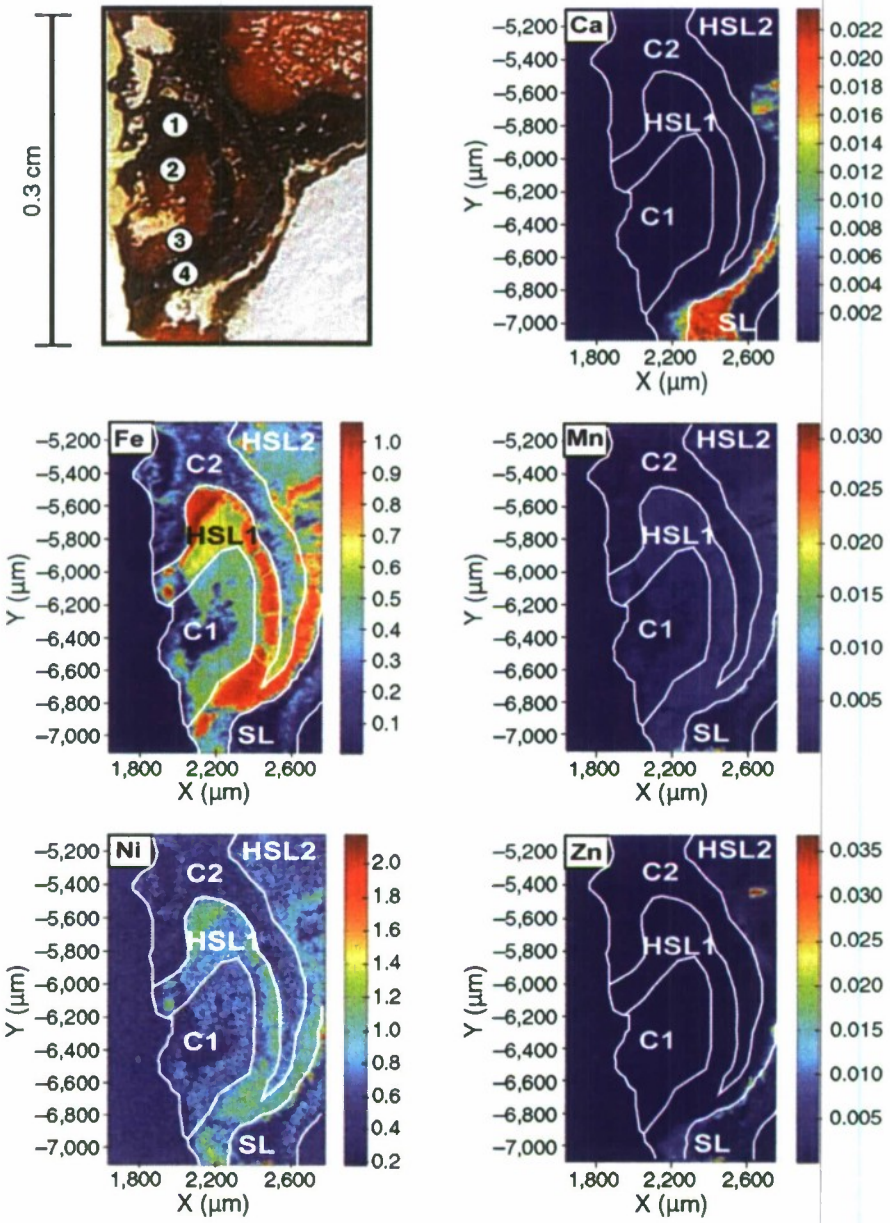

FIGURE 4. *µ-XRF maps of Ca, Fe, Mn, Ni, and Zn concentrations for a micro-sized classic mound-shaped iron corrosion product. The numbers indicate the locations of the representative µ-XRD traces. Core (C), hard shell layer (HSL), surface layer (SL).*

at cathodically produced gas bubbles (i.e., H_2). By physically separating the anode and cathode, Stone and Goldstein[26] generated tubular structures electrochemically in iron-ammonium sulfate solutions. The "ferrotubes" grew to millimeter size in tens to hundreds of minutes. In their work, hydrogen gas bubbles were covered rapidly with precipitating iron, creating a film that fractured and eventually slid onto the pipe surface creating the walls of a tube. They demonstrated that cathodic hydrogen gas production could provide the conditions for dynamic templating in a cast iron pipe. The iron oxides/hydroxides produced on the tube wall were arranged in the same oxidation sequence observed in the DWDS tubes.

It has been demonstrated[27] that both tubes (hollow whiskers) and mound-shaped corrosion products can form in the same pipe during stagnation and high flow, respectively. Both conditions are common in residential mains, service lines, and premise plumbing. Regarding tube formation, Butler and Ison[27] proposed, "Ferrous ions, formed at the anodic area at the root of the whisker, diffuse along the tube, and growth of the whisker proceeds at the tip, where these ions are oxidized and precipitated as iron oxide on coming in contact with the aerated water." Whiskers were up to 90 mm in length with growth rates more than 1 mm per day. Whisker diameter tapered from 0.4 mm at the base to 0.2 mm at the growing tip. The whiskers

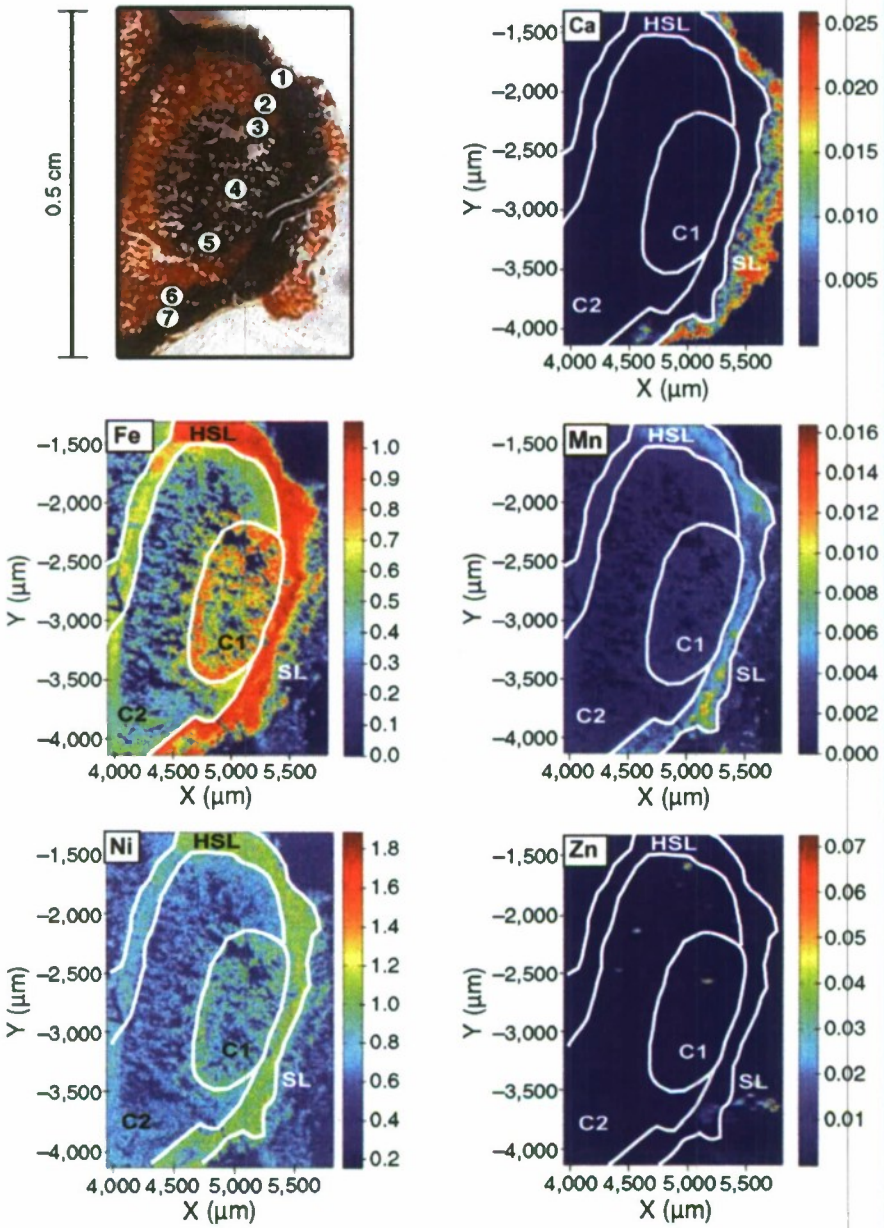

FIGURE 5. *µ-XRF maps of Ca, Fe, Mn, Ni, and Zn concentrations for a representative micro-sized tube shaped iron corrosion product. The numbers indicate the locations of the representative µ-XRD traces. Core (C), hard shell layer (HSL), surface layer (SL).*

were made up of goethite, magnetite, and a mixture of both.

As previously demonstrated in laboratory experiments,[26-27] the nature and location of the cathodic reaction can influence corrosion product morphology. Several cathodic reactions are possible in unlined cast iron pipes exposed to oxygenated, chlorinated drinking water. The most obvious potential cathodic reactions are reduction of water and O_2, resulting in H_2 and OH^-, respectively. In the absence of oxygen, it is possible for a previously deposited ferric scale to accept electrons from metallic iron ($Fe_{(metal)}$) as follows in the equation:[27]

$$Fe_{(metal)} + 2FeOOH_{(scale)} + 2H^+ \rightarrow 3Fe^{2+} + 4OH^- \quad (1)$$

Under oxygen-depleted conditions, McEnaney and Smith[28] suggested that FeOOH scale could be reduced to magnetite by a process of reductive dissolution as follows:

$$3FeOOH_{(scale)} + e^- \rightarrow Fe_3O_4 + H_2O + OH \quad (2)$$

Chimney features reportedly have served as vents for corrosion products (including H_2) on gray cast iron in water at 50°C.[10] Smith and McEnaney observed[10] that the chimneys formed under the crust and sur-

mised that acidic conditions developed under the crust similarly to acidic regions near pits in chloride solutions of comparable concentrations (100 ppm Cl^-).[29] Mankowski and Szklarska-Smialowska[30] established that increased acidity within pits was a consequence of significant Cl^- levels above the bulk solution content. Smith and McEnaney[10] proposed that under acidic conditions H^+ reduction (as opposed to water reduction in neutral conditions) would become the cathodic process within the accumulated corrosion products and O_2 reduction would occur on the nodule crust. They did not relate growth of the chimneys to dynamic templating.

CONCLUSIONS

❖ Mounds, mounds with protruding tubes, and free-standing tubes were identified as corrosion morphologies in a single 30 cm section of unlined cast iron pipe removed from a DWDS. Regardless of form or size, the physicochemical characteristics for all corrosion products were similar. Surface-bound microorganisms and minerals were eliminated as possible static templates due to their size relative to the tubes. Dynamic templating because of cathodic hydrogen production is suggested as a possible mechanism for tube-like corrosion product formation in unlined cast iron piping.

❖ It is proposed that in cast iron pipes exposed to aerated, chlorinated drinking water, metallic iron is oxidized to Fe^{2+} by dissolved oxygen in the water, released into the water and further oxidized to Fe^{3+}, forming $Fe(OH)_3$, which accumulates on the inner wall of the cast iron pipe at locations that are not necessarily associated with localized corrosion. The $Fe(OH)_3$ dehydrates and becomes FeOOH. Below a critical O_2 concentration, FeOOH is reduced to Fe_3O_4. Gas production at the cathode causes breaks (vents) in the crust. Growth of the vents into tubes is the result of templating on the cathodically produced gas bubbles. This proposed series of events has not been demonstrated in the laboratory under conditions that are relevant to a DWDS. However, the proposed cathodic reactions can be used to explain the consistent mineralogy among the shapes and sizes of corrosion products formed in DWDS with differing chemistries.

ACKNOWLEDGMENTS

PNC/XOR facilities at the Advanced Photon Source, and research at these facilities, are supported by the U.S. Department of Energy (DOE) – Basic Energy Sciences, a major facilities access grant from NSERC, the University of Washington, Simon Fraser University, and the Advanced Photon Source. Use of the Advanced Photon Source, an Office of Science User Facility operated for the U.S. DOE Office of Science by Argonne National Laboratory, was supported by the U.S. DOE under Contract no. DE-AC02-06CH11357. We thank S.A. Walley and J.B. Maynard for insightful comments on earlier versions of this paper, M.K. DeSantis for digital images of the iron corrosion products, and A. Lane (ELE, Inc.) for graphic support. The work at NRL was supported by ONR program elements 61153N, NRL/JA/7330-11-0717. The opinions expressed in this paper are those of the author(s) and do not necessarily reflect the official positions and policies of the USEPA. Any mention of product or trade names does not constitute recommendation for use by the USEPA.

REFERENCES

1. J. Lin, M. Ellaway, R. Adrien, *Corros. Sci.* 43, 11 (2001): p. 2065.
2. L.S. McNeill, M. Edwards, *J. Am. Water Works Assn.* 93, 7 (2001): p. 88.
3. P. Sarin, V.L. Snoeyink, D.A. Lytle, W.M. Kriven, *J. Environ. Eng.* 130 (2004): p. 364.
4. J.R. Baylis, *J. Am. Water Works Assn.* 15, (1926): p. 598.
5. H.M. Herro, "MIC Mythes—Does Pitting Cause MIC?," CORROSION/1998, paper no. 98278 (Houston, TX: NACE International, 1998), p. 278/1.
6. T.L. Gerke, J.B. Maynard, M.R. Schock, D.A. Lytle, *Corros. Sci.* 50, 7 (2008): p. 2030.
7. R. Ray, J. Lee, B. Little, T. Gerke, *Mater. Corros.* 61, 12 (2010): p. 993.
8. P. Ange, P. Angell, "Predictive Model for Non-Microbially Influenced Corrosion Tuberculation," Final Report EPRI Palo Alto, California, 2003.
9. H.M. Port, R.D. Port, *The NALCO Guide to Cooling Water System Failure Analysis* (New York, NY: McGraw-Hill, 1993), p. 37-65.
10. D.C. Smith, B. McEnaney, *Corros. Sci.* 19, 6 (1979): p. 379.
11. J.R. Baylis, *J. Am. Water Works Assn.* 45 (1953): p. 807.
12. J.B. Corliss, J. Dymond, L. Gordon, J.M. Edmond, R.P. Herzen, R.D. Ballard, K. Green, A. Bainbridge, K. Crane, T.H. van Andel, *Science* 203 (1979): p. 1073.
13. R. Ray, B.J. Little, "Environmental Electron Microscopy Applied to Biofilms," in *Biofilms in Medicine, Industry and Environmental Biotechnology*, ed. P. Lens, A.P. Moran, T. Mahony, P. Stoodley, V. O'Flaherty (London, U.K.: IWA Publishing, 2003), p. 331-351.
14. T.L. Gerke, K.G. Scheckel, J.B. Maynard, *Sci. Total Environ.* 408 (2010): p. 5845.
15. American Mineralogist Crystal Structure Database, http://rruff.geo.arizona.edu/AMS/amcsd.php, December 16, 2011.
16. D. Barthelmy, "Mineralogy Database," http://webmineral.com/, December 16, 2011.
17. R.M. Cornell, U. Schwertmann, *The Iron Oxides: Structure, Properties, Reactions, Occurrences, and Uses* (Weinheim, Germany: Wiley-VCH Verlag GmbH & Co. KGaA, 2003).
18. A. Hammersley, *ESRF* 10 (2001): p. 132.
19. P. Sarin, V.L. Snoeyink, J. Bebee, K.K. Jim, M.A. Beckett, W.M. Kriven, J.A. Clement, *Water Res.* 38, 5 (2004): p. 1259.
20. P. Sarin, V.L. Snoeyink, J. Bebee, W.M. Kriven, J.A. Clement, *Water Res.* 35, 12 (2001): p. 2961.
21. M. Sancy, Y. Gourbeyre, E.M.M. Sutter, B. Tribollet, *Corros. Sci.* 52, 4 (2010): p. 1222.
22. Z. Tang, S. Hong, W. Xiao, J. Taylor, *Corros. Sci.* 48, 2 (2006): p. 322.
23. D.A. Lytle, T.L. Gerke, J.B. Maynard, *J. Am. Water Works Assn.* 97, 10 (2005): p. 109.
24. H.F. Ridgway, B.H. Olson, *Appl. Environ. Microbiol.* 41, 1 (1981): p. 274.
25. H. Hashimoto, S. Yokoyama, H. Asaoka, Y. Kusano, Y. Ikeda, M. Seno, J. Takada, T. Fujii, M. Nakanishi, R. Murakami, *J. Magn. Magn. Mater.* 310 (2007): p. 2405.
26. D.A. Stone, R.E. Goldstein, *Proc. Natl. Acad. Sci. U.S.A.* 101 (2004): p. 11537.
27. G. Butler, H.C.K. Ison, *Nature* 182 (1958): p. 1229.
28. B. McEnaney, D.C. Smith, *Corros. Sci.* 20 (1980): p. 873.
29. G. Butler, H.C.K. Ison, A.D. Mercer, *Br. Corros J.* 6, 1 (1971): p. 31.
30. J. Mankowski, Z. Szklarska-Smialowska, *Corros. Sci.* 15 (1975): p. 493.